HYPERVELOCITY DEBRIS INITIATED SPACECRAFT DISCHARGING

Charles Stein
U.S. Air Force Research Laboratory
Space Vehicles Directorate
2050 Chanute Street
Kirtland Air Force Base
Albuquerque, New Mexico, 87117
USA
charles.stein@kirtland.af.mil

1. INTRODUCTION

The effects of spacecraft charging can produce serious operational anomalies due to arc-discharging and its production of electromagnetic fields which couple into spacecraft electronics. In addition, the discharging produces localized heating and ejection of surface material which can be a source of contamination for other spacecraft surfaces. While it is generally recognized that electrostatic discharge (ESD) results from a localized buildup of charge differential on the spacecraft surface, to the point of the breakdown threshold of the material, there is evidence that other initiators of arc-discharging must occur. This is because spacecraft outages have taken place at geomagnetic quiet times or on the day-side of the spacecraft, remote from enhanced electron fluxes[1]. Moreover, since there is often a long delay between charging and subsequent discharging[2], which requires a continued absence of cold plasma ions, the question of what constitutes the discharge trigger mechanism is raised. Electrostatic discharge from deep charging of dielectric materials offers an alternative explanation[3], but no conclusive patterns of cause and effect have been established. On the other hand, some researchers have suggested that hypervelocity debris could play a role in triggering electrostatic discharging.

This paper presents the results of hypervelocity debris impact experiments on spacecraft materials and offers the suggestion that this phenomenon may provide an alternative mechanism for triggering ESD.

Spacecraft placed in low-Earth orbit (LEO) are exposed to a large flux of hypervelocity impacts by small particles which originate from micro-meteorites and man generated debris[4,5,6]. At additional risk are proposed large inflatable space structures, as well as multiple satellite constellation systems because of the possibility of collateral damage. The amount of damage experienced by space based assets in LEO from hypervelocity debris impacts can be extensive and can decrease the performance levels of subsystems below critical specifications. In LEO, the particle flux existing in circular orbits at altitudes near 500 kilometers[7] varies between 10 and 100 hits /m^2/yr. for sizes of about 0.1 mm and smaller, which is the range of sizes of interest in producing ESD. The damage generated by the larger of these debris particle on impact can be grouped into three distinct phenomena: a) mechanical property changes due to cratering (which is often many times larger in diameter than the particle itself) and surface damage produced by direct hits; b) internal and back surface spallation of materials resulting from the shock wave produced by the hypervelocity impact; and c) molecular and particulate contamination which arises from the vaporization of the impacting particle itself as well as that of the material struck. Hypervelocity debris particles, moving at relative velocities near 10km/sec in LEO, generate temperatures[8] in the range of 5,000 ^{0}K and pressures of several megabars on striking a surface and produce a plasma of charged and neutral non-stoichiometric molecules of the decomposed constituents of the spacecraft surface, as well as molten droplets. The morphology of contaminant examined in the previous work cited[8] by transmission electron microscopy, where pulse laser simulation of hypervelocity debris impacts of a composite matrix resin were carried out, produced sub-micron size, single crystal platelets of graphite. Because of the extremely high temperatures and pressures produced on impact, many of the reaction products are not the same as those produced under ambient conditions where reactions are expected to proceed by the Rice-Herzfeld mechanism.

The nature of the blow-off produced by hypervelocity debris impacts on protective glass covering solar cell panels, which is reported in this work, serves as an example of a mechanism which could trigger ESD. Since the area of solar panels represents a large fraction of a satellite's charged surface, this work may provide some particularly relevant information regarding alternative ESD triggering mechanisms. In addition, since much of the man-made debris in LEO are metallic particles, the aluminum foil used as debris in these experiments probably represents typical space damage to spacecraft.

2. EXPERIMENTAL

The technique used in this work to accelerate debris particles to near LEO relative velocities has been described, in detail, by Roybal et al, elsewhere[9]. Therefore, only a summary of the salient points are mentioned here. The method used to fabricate the debris particle/launching system is critical to producing the acceleration desired. In the method which we have developed, a metal foil of the desired thickness for the debris particle is tenaciously bonded to a glass substrate by atomic diffusion of the metal into the glass. Both elevated temperature and a DC voltage are applied across the metal/glass laminate to produce a very strong and uniformly bonded interface.

The metal foil is struck by a laser beam which is focused through the thin sodium glass disc and starts to vaporize the foil at the glass/metal interface. A neodymium-glass, pulsed laser with energies ranging from 2 -5 joules and a 18 ns pulse was used in this work. The vapor pressure thus produced reaches levels in the giga Pascal range which cuts out and accelerates a small metal disk, the diameter of the periphery of the laser beam. Using this technique, velocities from 4.5 to 7.5 km/s have been achieved. This compact method for impacting spacecraft materials at hypervelocities is carried out in a space environmental effects chamber which has the additional capability of exposing samples, simultaneously, to energetic electrons, ultraviolet radiation and atomic oxygen. In the work reported here, impact testing was carried out on solar cell cover glasses using flat aluminum debris particles, 3mm in diameter and 3 microns thick. The cover glass targets, which were 4.0cm by 4.0cm in size, consisted of two thin glass sheets laminated together with a thin layer of Teflon or CV2500 resin between them. The debris particles, which traveled a distance of approximately 12 mm before impacting the target, had their velocities determined by a laser interferometer system[10] in which a small Doppler shift in the frequency of the laser beam, returned from the surface of the moving debris particle, is measured. Only one hit was made per target so that an assessment of the amount of re-deposited ejecta from a single impact could be determined. The damage observed in these experiments included: front surface cratering; front and rear-surface radial and concentric cracks; rear-surface uplift; and spall. In addition, molten and solid contamination from material vaporized and ejected from the crater was re-deposited on the front surface of the cover glass. Mechanical damage to the targets was characterized using optical and scanning electron microscopy (SEM) with fluorescent elemental analyses of the ejecta.

3. RESULTS

Figure 1 shows a typical optical micrograph of an impacted coverglass target in which the mechanical damage resulted from a 3mm diameter particle impacting at 4 km/s. Radial cracks extend from the impact crater to the edge of the 4 cm sample. The circle in the center of the image represents the size and impact location of the 3 mm debris particle.

Fig. 2 is a schematic diagram of the impacted sample shown in Fig.1, where an interesting disposition of the deposited ejecta from the impact crater onto the target surface is seen. The ejecta forms bands of different materials and densities radiating out from the crater area. In this diagram, (A) represents the size of particle impacting the surface; region (B) is the crater area in which material has been removed from the target; area (C) contains molten aluminum which is also found covering the entire sample in the form of trace deposited vapor; area (D) remained relatively free of contaminate deposition; and in area (E), at a distance of over 1 cm from the impact site, the surface is heavily coated with deposited organic vapor removed from the sheet bonding the two cover glasses together.

An elemental analysis of the coverglass surface was completed using an energy dispersive system attached to our scanning electron microscope and produced the qualitative analysis shown in Figures 3, 4 and 5.

Figure 3 shows the spectrum of the surface of a "control" sample which consists primarily of silicon and potassium for a glass that has not been impacted. Figure 4 is an energy dispersive spectra of the impact crater, area (A). In the crater area much of the glass has been removed, revealing the resin layer below which produces the resulting fluorine and carbon lines with reduced intensities of Si and K. The energy dispersive spectra in Figure 5 was collected from area (E) and shows the presence of carbon, fluorine, silicon and aluminum.

In the previous work cited[8] the chemical characteristics of the vaporized species were determined, in situ, by time-of-flight mass spectroscopy. Those analyses showed that many of the species vaporized were positively charged molecules. This is mentioned here since scanning electron microscopy energy dispersive chemical analyses does not distinguish between charged and neutral species.

.

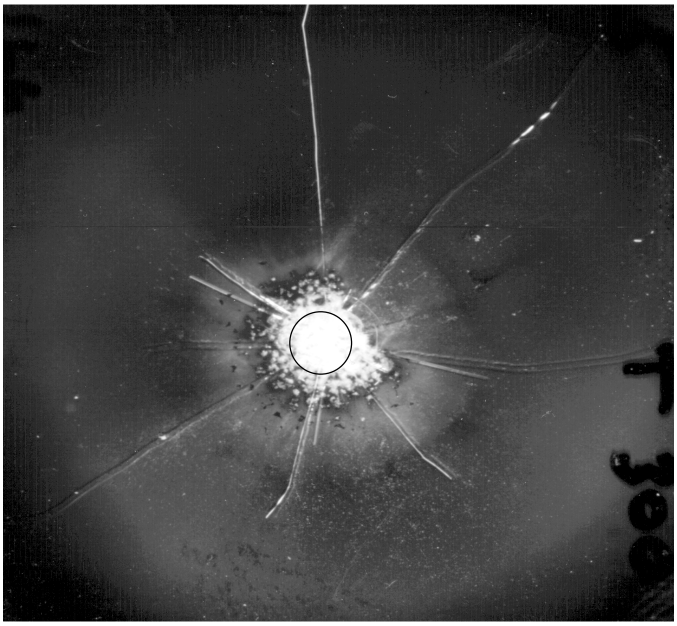

Fig. 1. 4X optical image of a coverglass laminate impacted with a 3mm particle at 4 km/s.

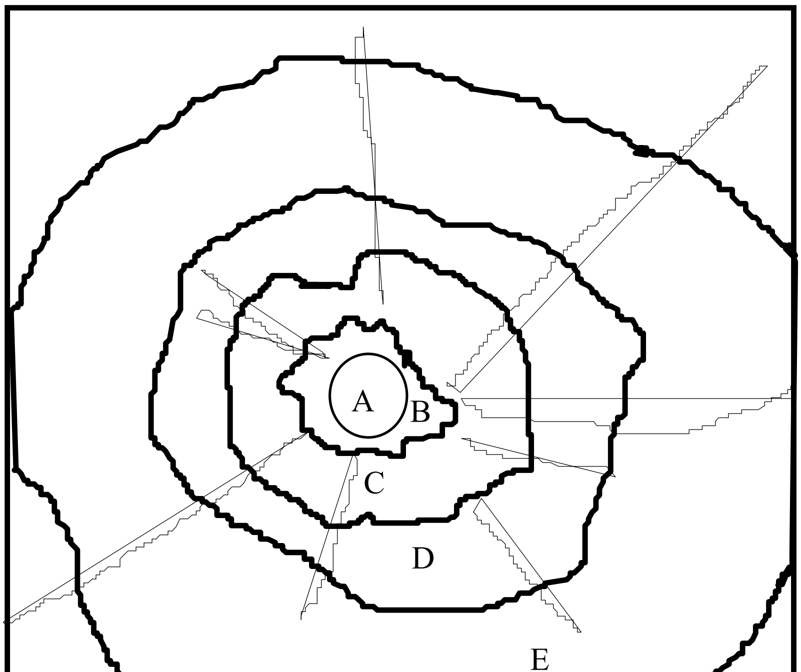

Fig. 2. Schematic of the impacted area of Fig. 1 showing outlines of re-deposition regions.

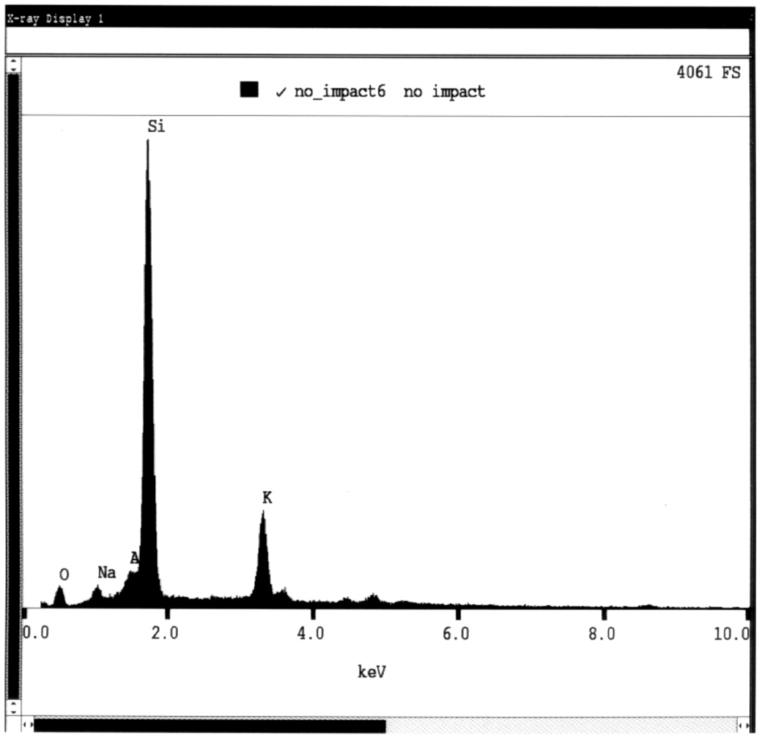

Fig. 3. Energy dispersive spectrum of the surface of a non-impacted coverglass.

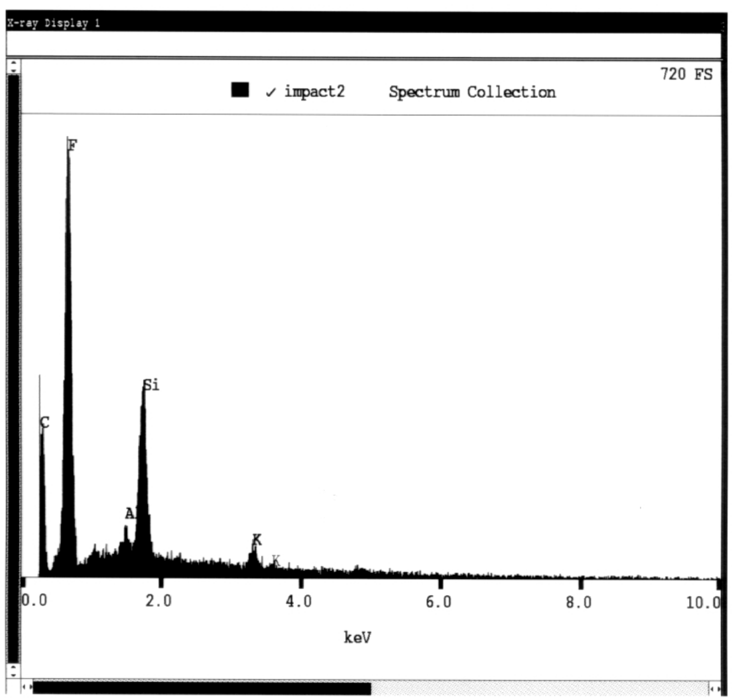

Fig. 4. Energy dispersive spectrum of the crater area (A) of Fig. 2 on impacted coverglass.

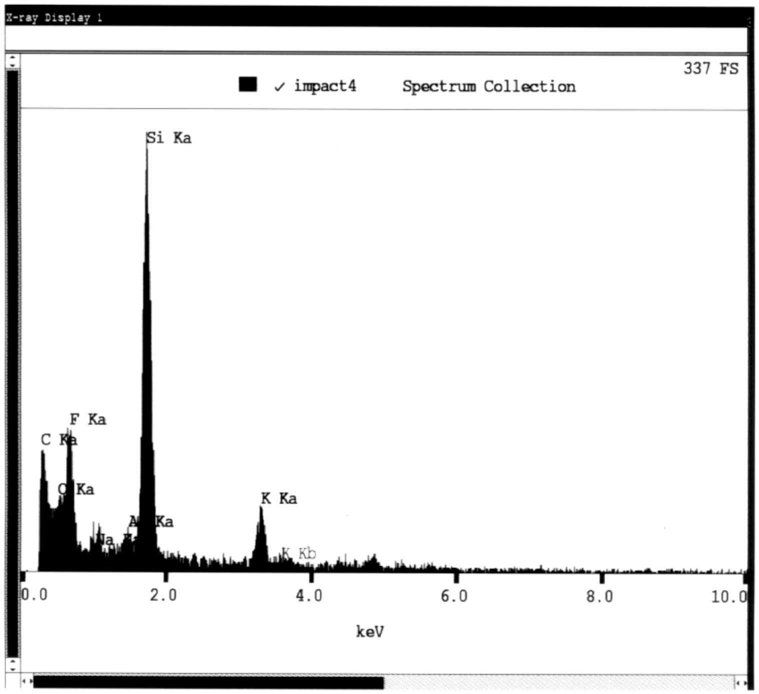

Fig. 5. Energy Dispersive spectrum of area (E) of Fig.2 on impacted coverglass.

The above spectra show that a deposition of fluorine, carbon, and aluminum are now present in regions of the impacted cover glass. The fluorine and carbon are generated from the vaporization and ejecta of the Teflon or CV2500 resin layer of the laminate. The source of aluminum comes from vaporization of the aluminum debris particle.

4. DISCUSSION AND CONCLUSIONS

Results are presented of experiments conducted to determine the nature of the plasma produced by the impact of hypervelocity debris particles on a spacecraft sub-system and the possibility that they could constitute a triggering mechanism for ESD. Hypervelocity impacts produce damage in the form of cratering, ejecta of the solid constituents of the surface, a plasma consisting of the cover glass laminate material and vaporized aluminum from the impacting particle. The morphology of the deposited ejecta and the chemistry of the vapor were determined by scanning electron microscopy and energy dispersive spectroscopy. The vapor products of the ejecta were spread over a rather large area compared to the diameter of the debris particle, as over 90 percent of the 4.0cm by 4.0cm sample was covered with a deposition of the contaminant film. (Subsequent experiments have shown that this film produced a 15 percent loss in light transmission through the solar cell cover glass, over solar wavelengths of interest.)

From these finding, it is suggested that hypervelocity debris or micrometeorite impacts on spacecraft with differentially charged surfaces could constitute a mechanism by which electrostatic discharging could be triggered. This mechanism may explain the discharge anomalies noted on spacecraft surfaces, especially those occurring on the day-side of the spacecraft and during geomagnetic quiet times.

5. ACKNOWLEDGEMENT

The author wishes to thank Robert Roybal and Pawel Tlomak, of the US Air Force Research Laboratory, for their extensive contributions to this research and for their many enlightened discussions of the results.

REFERENCES

1. G. Wrenn and A. J. Sims, “Spacecraft Charging In Geosynchronous Orbit”. NATO Advanced Study Institute Proceedings, Pitlochry, Scotland, July 7-19, 1991
2. H. Lam and J. Hruska, “Magnetic Signatures For Satellite Anomalies”. J. Spacecraft, 28, pp.93-99, 1991.
3. A. J. Coates, A. D. Johnstone, D. J. Rodgers and G. L. Wrenn, “Quest For The Source Of Meteosat Anomalies”. Proceedings of the Spacecraft Charging Technology Conference”. Monterey, California, pp120-146, 1989.
4. E. Schneider, “Micrometeorite Impact On Solar Panels. Proceedings of the 5th European Symposium: ‘Photovoltaic Generators in Space’, Scheveningen, The Netherlands, 30 September, 1986.
5. F. M. Rose, “Hypervelocity Impact On Solar Cells”. NASA Technical Report, NASA-CR-192444, January, 1993.
6. H. Dursch, “Results From Testing And Analysis Of Solar Cells Flown On LDEF”. Proceedings of the LDEF Materials Workshop, NASA/Langley, Part 2, pp. 649-660, September 1992.
7. D. J. Kessler, R. C. Reynolds and P. D. Anz-Meador, “Orbital Debris Environment for Spacecraft Designed To Operate In Low Earth Orbit". NASA-TM 100471, September, 1988.
8. R. Roybal, C. Stein, C. Miglionico and J. Shively, “Laboratory Simulation Of Hypervelocity Debris”. Int. J. Impact Engineering, vol. 17, pp. 707-718, 1995.
9. R. Roybal, J. Shively, C. Stein and C. Miglionico, “Proceedings Of The 19th Space Simulation Conference”, NASA Conference Publication 3341, Baltimore, MD, October 28-31, 1996.
10. L. M. Barker and R. E. Hollenbach, “Laser Interferometer For Measuring High Velocities Of Any Reflecting Surface”, J. Appl. Phys. 43, pp. 4669-4675, 1972.

Risks of low voltage arcs sustained by the photovoltaic power of a satellite solar array during an electrostatic discharge. Solar Arrays Dynamic Simulator

D. Payan , D. Schwander*, J.P. Catani*
Denis.payan@cnes.fr
* Centre National d'Etudes Spatiales
Département Alimentation & Compatibilité Electromagnétique
18, avenue Edouard BELIN
31401 TOULOUSE Cedex 4 FRANCE

Abstract –The validation of new solar cell for geostationary satellite use sets the problem of arcing between solar cells triggered by electrostatic discharges (ESD). Tests have been carried out on GaAs solar array samples representative a French telecommunication satellite. The main difficulty of this test is to properly simulate the transient functioning of one string during the first microsecond of an electrostatic discharge. The CNES Solar Simulator with all the physical data we need to take into account to properly simulate de functioning of the string.

The solar simulator was designed and produced at CNES. The electrostatic discharge vacuum tests triggered by thruster ignition were conducted at ONERA/DESP in TOULOUSE in the JONAS vacuum chamber during the CNES R&T.

Chapitre 1. Introduction

In the laboratory, the ESD tests on solar array samples set the problem of the representativity in relation to the real flight configuration. Indeed, we have a sample of only several cells whereas we should effectively represent a string or even a complete section of a solar array in the process of supplying power.

In the secondary arc case, the energy is supplied by the cells themselves and the string outputs into the arc when the cells are illuminated. To conduct a representative test, we must therefore have SA voltage (to simulate the pd between two adjacent cells at the end of the string), but also the nominal current circulating in the cell diodes (this represents the case where the solar array is in open circuit configuration and outputs to the cell diodes) capable of tripping to short circuit configuration in several microseconds.

As the primary discharge lasts only few microseconds, the response time of the system must be several hundreds nanoseconds. But, the best power supplies switch from voltage regulation to current regulation in 50 to 60µs. Also, the output capacitance of a laboratory power supply is generally several hundred microfarads to be compared with the value of around 500nF for an SA string. The overvoltage at the time of the secondary arc is then too high eliminating the representativity of the test.

We therefore had to find a simple device, using the laboratory power supplies, which could deliver any current and any voltage in several microseconds.

It is with this in mind that we produced a Solar Array Simulator (**SAS**) using 4 power supplies and a simple connection box including diodes (see photos).

Chapitre 2. The risk

On account of their complexity, there is always an electrostatic risk on Solar Arrays (SA). In the event of an ESD (ElectroStatic Discharge), the integrity of the solar array is generally not affected during this discharge. The EMC risks remain however high for the satellite as a whole. But, with the increase of the power of the Solar Arrays, we have seen the appearance of low-voltage arcs sustained by the photovoltaic power of the solar array (**secondary arcs**). These breakdowns have occurred between two adjacent cells generally those at the start and the end of the cell string where the voltage is maximum. The propagation of the current in the inter-cell vacuum is made possible in the plasma generated by the **primary discharge (**ESD). The secondary arc probably exists for each ESD when it appears in a gap between twi cells and reflects the circulation of a leakage current between the cells, in the primary discharge conductive plasma. However, whilst the current-voltage values are relatively low (typically 2A-50V), this discharge remains transient, does not lead to irreversible effects and remains therefore "invisible" to the experimenter.

The energy contained in a primary discharge comes from the electrostatic energy stored during the charging of the materials by electrons from the environment. It is low when compared with the secondary arc energy which comes from the solar array itself when it is illuminated.

We speak therefore of the primary discharge (trigger arc) for the electrostatic discharge and the sustained arc when the arc is generated between adjacent cells.

If the solar array has no blocking diode on each cell string, the complete section can output into the conductive path between cells increasing the short circuit risk. In failure cases, the complete section is lost.

Chapitre 3. Solar cell sample

A - Description

The sample tested is a sample including 2 rows of 3 Gallium Arsenide solar cells in series

The composition of a cell is as follows:

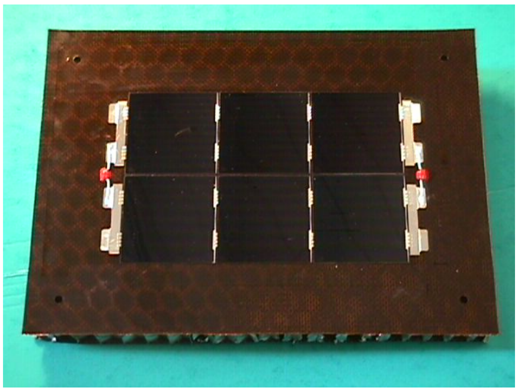

Fig 1: Photograph of solar cells sample – Front face.

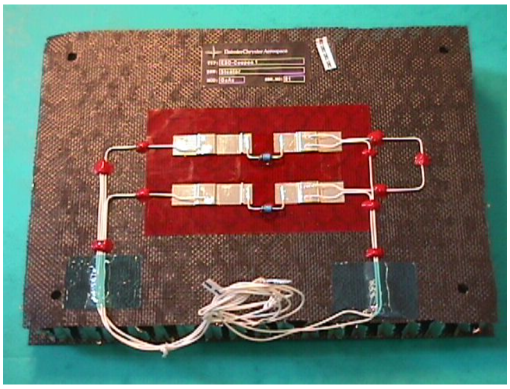

Fig 2: Photograph of solar cells sample – Rear face.

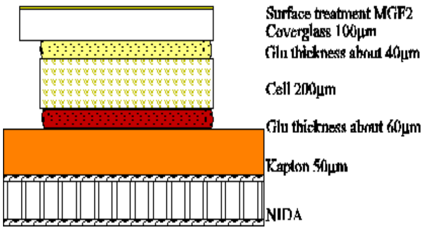

Fig 3: Cross-sectional view of a solar cell

B - Spacing between cells

The spacing between the cells is not constant as the assembly is done manually. It has been measured on the sample at various locations and is generally between 800 and 900µm.

Chapitre 4. .The Dynamic solar array simulator

A - Simulation of the power delivered by the solar array itself

1 - Principle

The cell current is imposed by a current source outputting via the cells.

The string voltage is obtained by inserting a resistor (variable in order to test several values and possibly search for the critical threshold) between the two cell strings.

All the power supplies are protected by 10A diodes (BYW 78200M, except for Istring and Vsection: BYW 92200).

Thus, by varying the resistance, and as we impose the current, we vary the voltage between cells.

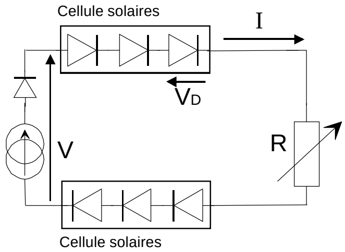

$V = R \bullet I + 6 \times V_D$
V = Tension Bus
R = Résistance variable
V_D = Tension Diode

Fig 4: Sample polarisation principle.

Unfortunately, such a device has the drawback, in the secondary arc cases, of always sharing the current available (that of the current source) between the arc and the resistor. As the arc is resistive (typically around ten ohms), for conventional current-voltage values, the current continuing to circulate in the resistor R remains non negligible. We therefore do not have the maximum current available in the secondary arc.

We therefore had to find an electronic trick to get round this drawback.

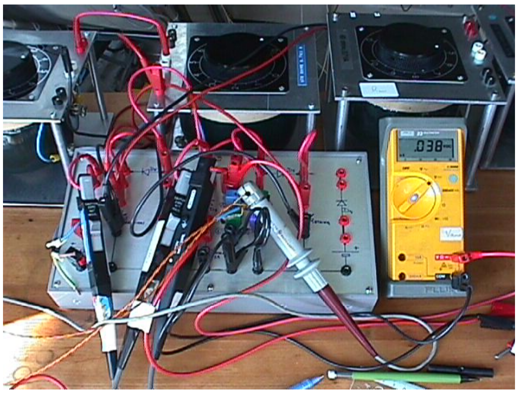

Fig 5: Photos of solar simulator.

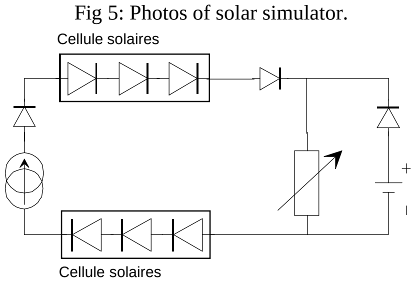

Figure 6: SA simulator device.

The system used is that of a diode switch. Using a voltage source, we maintain, at the terminals of the resistor, a voltage slightly lower than the normal voltage due to the polarisation (the voltage source therefore does not output in normal operating case) and everything happens as in previous case except for the voltage drop in the diode.

$$V_{RSTRING} = R_{STRING} \bullet I_{STRING} - e$$

This diode is normally polarised while there is no short circuit.

The same principle is adopted for the section current. We add an additional loop to simulate the current of a solar array section. A diode (D2) blocked in normal operation, prevents it from outputting to the string, whereas a diode (D1), at that time conductive, imposes a path via the resistor Rs (which is also used to adjust the section current from the bus voltage).

We are therefore in a situation where we have the string current through the cells and a current available in secondary arc cases which is pending in an adjacent loop.

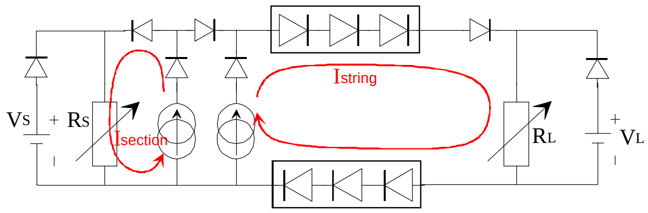

Fig 7: The string and section current without secondary arc.

In secondary arc cases, there is a voltage drop at the end of string cell and the polarities at the diodes are reversed, the conductive diodes block and the blocked diodes become conductive. The situation is then as follows:

D1 blocked; D2 conductive;; D3 blocked

The String and Section currents are then naturally directed towards the location of the secondary arc. The advantage of such a process is that the current becomes available with the rapidity of the diode switching time (several microseconds). We must however make sure that the power supplies are already at current limitation when they output into the adjacent loop (see comparison between "correctly adjusted" and "poorly adjusted" power supply). If there is no such device, we would have to take the power supply "power-up" time into account (our measurements gave more than around fifty microseconds for the best), which is too long compared with the almost instantaneous availability of the power in the real case.

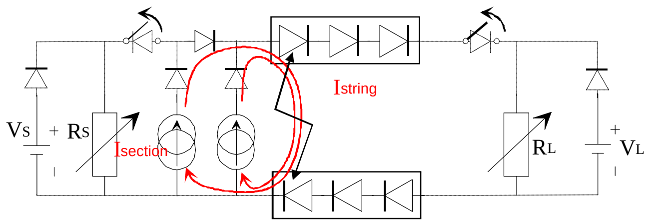

Fig 8: String and section currents at time of secondary arc.

Lastly, once the diodes are blocked, the voltage sources start to output into the resistors. This can be a means for checking the permanence or not of the short circuit.

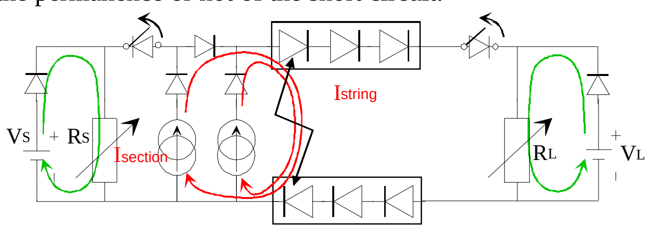

Fig 9: String and section currents after secondary arc.

From a technical viewpoint, the two resistors must be capable of absorbing the power required (50W for example if we want 50V and 1A) and the diodes must be sized to support several amps.

2 - CNES SAS – Standard power supply – HP SAS comparison.

To test the response times of the various power supplies, we adjust their voltages to 50V and have them output 1A into a 50Ω impedance by imposing a current limitation of 3A. Suddenly, using a mercury switch (to avoid rebound), we short circuit the 50Ω impedance with a 1Ω impedance. The power supplies then switch from voltage limitation state to current state and we plot the curve. We therefore see the current pass from 1A to 3A. For the experimentation, the transition must be made in several microseconds. For the CNES SAS, we make it output into the adjacent loop, already limited in current and the short circuit enables it to switch to 1Ω thus changing the current in the 1Ω resistor from 0 to 3A.

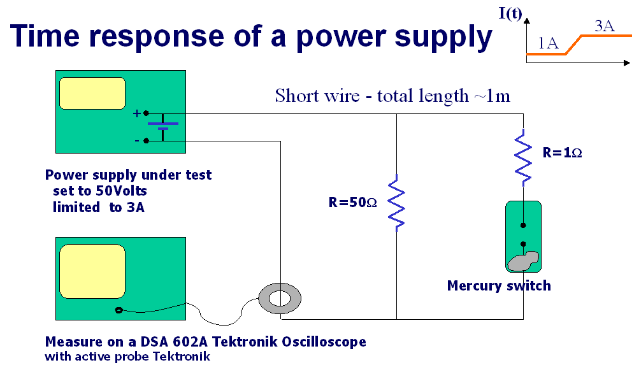

Fig 10: Time responses of a power supply test set-up.

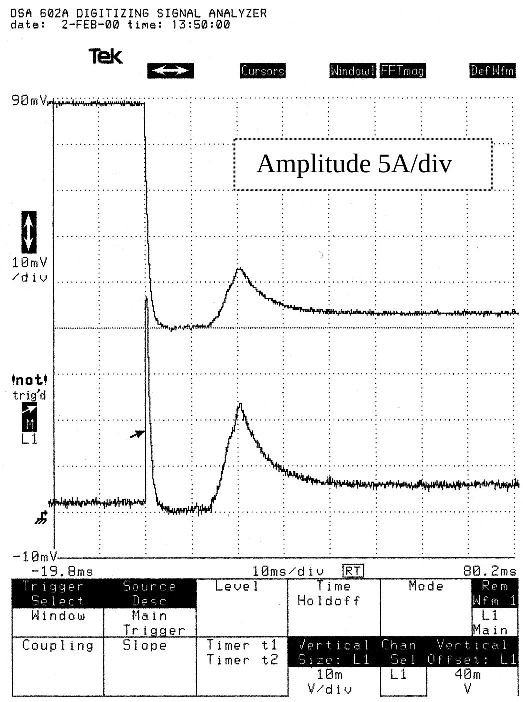

Fig 11: XANTREK XRH 150V-6A switched power supply.

On the transient, the XANTREK switched power supply trips out then restarts and limits the current in 40ms.

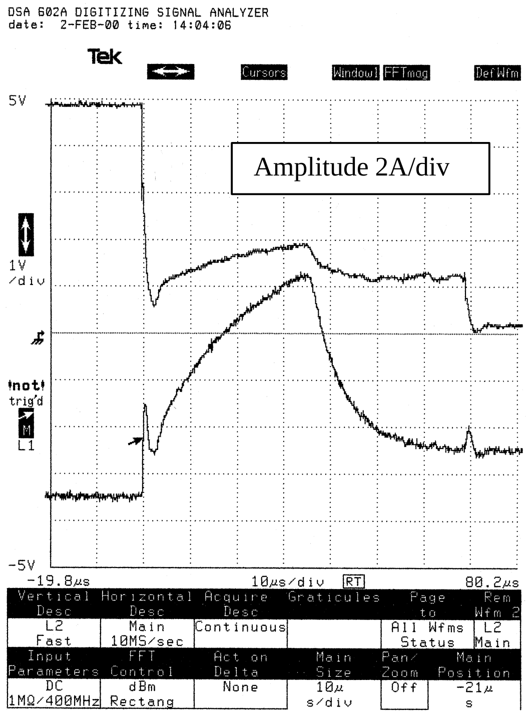

Fig 12: Hewlett Packard SAS E4350A power supply.

Thanks to its low output capacitance, the HP SAS achieves the current limitation in 60µs which is still too long for our experimentation.

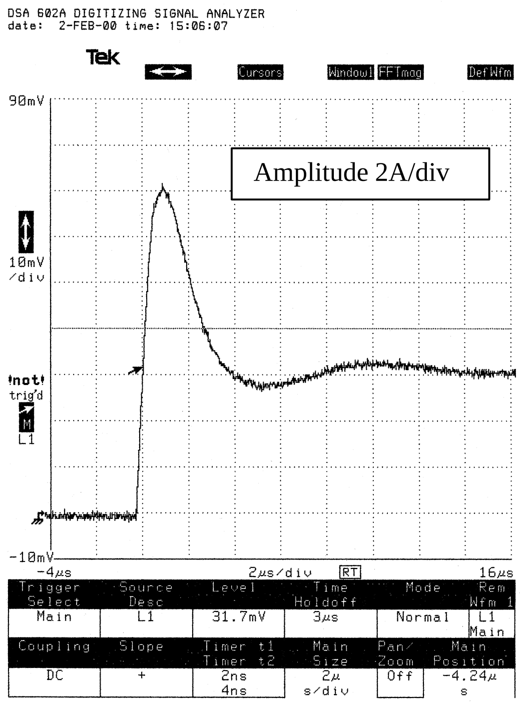

Fig 13: CNES SAS adjusted in current.

The CNES SAS must have its power supply already limited in current to avoid power supply response times which are too long. We thus obtain a limitation in 4µs with a reasonable overvoltage.

B - Electrical simulation of the power stored in the differents capacitances on the SA

1 - Introduction.

We know now, how to reproduce the energy delivered by the solar array itself during the discharge transient

With only 2 to 6 cells for the tests, we must take into account the energy that would have been stored in the different capacitances of the missing cells to be representative of a whole string. In order to have a test set-up as simple as possible, the energy stored in the whole string must be represented by only some few capacitances.

The schematic diagram is given below.

Must be considered :

- The absolute capacitance of the satellite C_{SAT}
- The capacitance of the string itself Cstring diff

This is the differential mode capacitance measured between the (+) and the (-) wire of the string.

- The Capacitance underneath the cells through the Kapton

This is the common mode capacitance measured between the (+) and the (-) wire of the string on one hand and the solar panel structure on the other hand. Cstring com

- The coverglass capacitance C_{ε}

This is the capacitance measured between the top of the cell and the top of the coverglass.

So, it is possible to be representative of the string behaviour with only four capacitances.

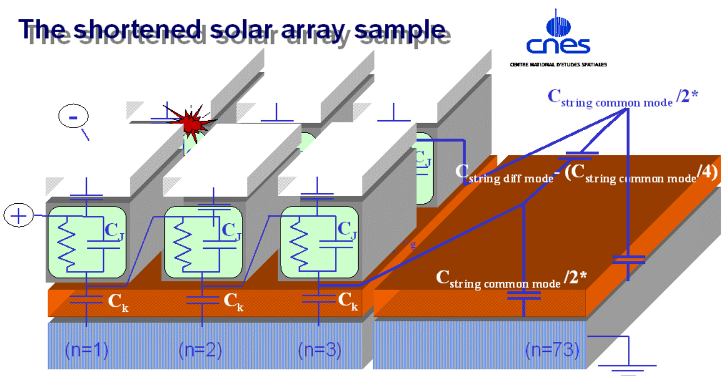

Fig 14: The shortened solar array sample
and the missing capacitances

2 - How to calculate elements.

a - The absolute capacitance of the satellite

Although we know today that the satellite capacitance plays a role of prime importance in the control of the inverted voltage gradient discharge and that its value is low (typically 300pF) (Ref[1]). We now know that the representativity is achieved by taking into account the true capacitance value of the satellite without adding the capacitance of the coverglasses.

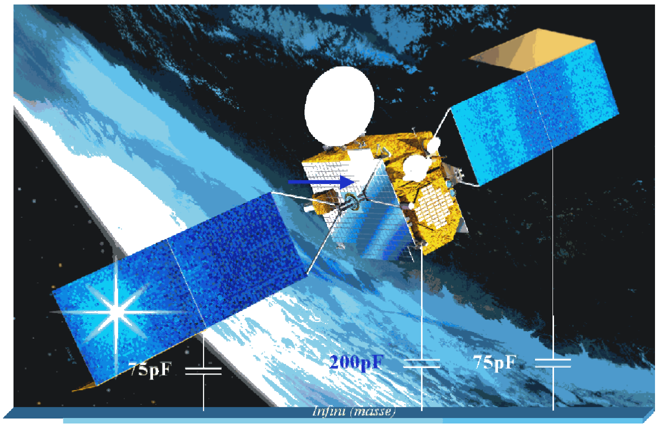

Fig 15: Absolute capacitance of the satellite

The difference with previous models and set-up lies in the way in which the energy contained in the coverglass capacitance is released. In our setup, as in flight situation, it is the Csat capacitance which controls the Coverglass capacitance discharge current in the same way as a transistor (for more information, see Ref[1 &3]).

b - *The Kapton capacitance for one cell*

This is the capacitance under the cell across the Kapton layer sheet and the bond. In the case of our French telecommunication satellite, the bond is 60µm thick and Kapton is 50µm thick. We must take into account the serial two capacitances.

$$C_k = e_0 e_r \cdot \frac{S(m^2)}{e(m)} en(\mu F)$$

$C_{kapton\ alone}$ = 900pF
$C_{kapton+glue}$ (estimated) = 450pF
$C_{kapton+glue}$ (measured) = 360pF C_k=15pF/cm²

Be careful to the value : Measurements must be done with a network analyser.

c - *The differential mode string capacitance (Réf[6]).*

This capacitance allows us to simulate the whole capacitance of the missing cells chain by only one capacitance between the (+) and the (-) wires. In the case of a floating solar array structure (during transients, when there is a bleeder resistor), we can write :

$$C_{String\ diff}(V_S) = \frac{1}{2} \cdot N_p \cdot \frac{\sqrt{C_k \cdot Cj(v)}}{th\left(\frac{N_S}{2} \cdot \sqrt{\frac{C_k}{Cj(v)}}\right)}$$

C_k = Capacitance through the kapton fo one cell
C_J = Junction capacitance for one cell
V_S = String voltage
v = Cell voltage = $\frac{V_S}{N_S}$
N_S = number of cells for one string
N_P = Number of string

We need to take the right value of the Cell junction capacitance due to its non-linearity (estimation of the capacitance for voltage values between 0 et Vnominal).

$$C_J(v) = C_{Ttransition} + C_{Diffusion}$$

$$300nF \langle C_{Transition} \langle some\ mF$$

$$some\ mF \langle C_{Diffusion} \langle some\ hundreds\ mF$$

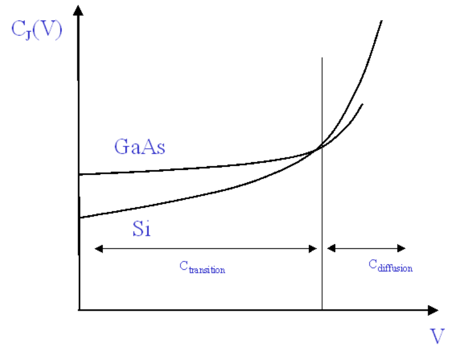

Fig 15: Junction capacitance of a cell versus to voltage

For high value of C_J : $\frac{N_s}{2} \cdot \sqrt{\frac{C_J}{C_k(v)}} \langle 1$

then, $\boxed{C_{string\ diff} \approx \frac{C_J(v)}{N_s}}$

As there is about one hundred cell per string, you must have $C_c \rangle 2500\, C_s$. This is the case when C_{MC} is negligeable, the equivalent capacitance of all a string correspond to the serial of the capacitances of each cell (C_c).

In the case where $\frac{N_s}{2} \cdot \sqrt{\frac{C_J}{C_k(v)}} \rangle 1$ then

$$\boxed{C_{string\ diff} \approx \frac{1}{2} \cdot \sqrt{C_J(v) \cdot C_k}}$$

d - *The capacitance through the Kapton for the missing cells ($C_{string\ com}$)*

We need to evaluate the capacitance between the string and the structure through the Kapton. $C_{string\ com}$ is choosen at is higher possible value which is $C_{String\ mod} = Np \cdot N_s \cdot C_k$.

This is a worst-case (the right value is below), but theoretical calculation shows us that this approximation is correct.

e - *The capacitance of coverglass*

$$C_e = e_0 e_r \cdot \frac{S(m^2)}{e(m)} en(\mu F)$$

This capacitance is evaluate for each coverglass

In fact it is hard to insert it in the test set-up.

It seems that we do not need more coverglasses than those which are available on the sample under test.

Be carreful, we cannot add this capacitance to the satellite capacitance. We cannot use a metallic electrode and we need to use a large enough dielectric for tests (4 to 6 cells seems to be enough). Experiments showed us that when a small satellite capacitance is used (the geostationary case), only the nearest area of coverglasses around the ESD is discharge.

C - Others elements

1 - Inductance

All connecting wires used in the test set-up set inductances, which slow down rise time of current available for the secondary arcing. They must be representative of the flight configuration.

2 - Inductances & Resistances effects

The insertion of a resistance in the loop of the secondary arcing allows to sustain the arc. Be careful to have electrical elements representative of the flight configuration.

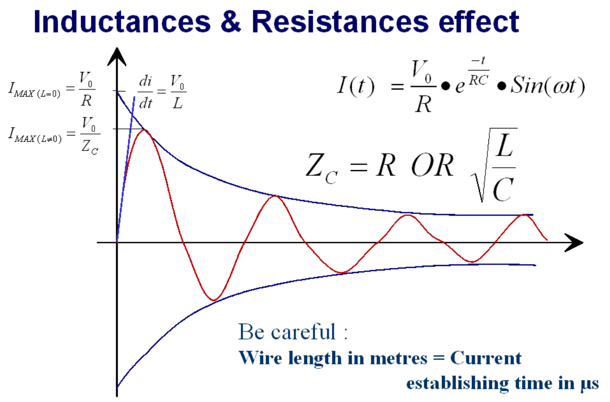

Fig 16: Discharging circuit oscillations

Critical damping condition if

$$R > 2\sqrt{\frac{L}{C}}$$

Inserting a resistance avoids underdamping in the oscillating circuit and consequently avoids stopping the secondary arcing. (Its increase R with respect to L.)

To be realistic we need to take into account :

- the resistance of one string only
- the inductance of this string.

And we must let the arc disconnecting if it is realistic.

If there is an added resistance to the discharging circuit, it will also affect the functioning point on the discharge curve.

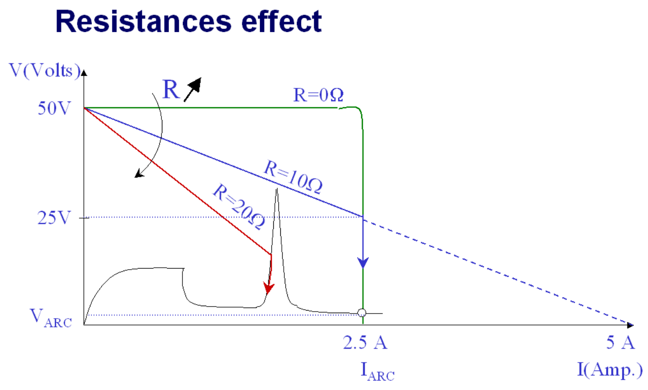

Fig 17: Effect of an added resistance in the circuit

D - The solar panel simulator device

The complete test set-up is presented below.

With such a device, it was possible to conduct electrostatic discharge tests in normal situation (the sample structure is connected to the ground and the dielectrics are charged) or in inverted voltage gradient mode.

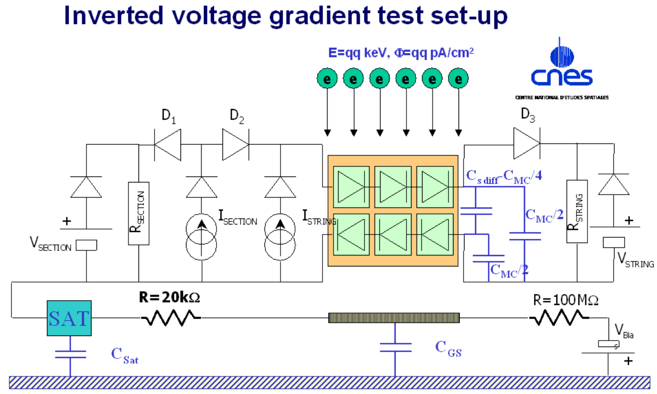

Fig 14: Setup simulating the satellite

Under certain environmental conditions, the satellite is charged negatively to several kilovolts and the resulting discharges are discharges of metallic origin when the structure discharges. In a laboratory, the representativity of such discharges is obtained by polarising the structure of the samples between –3500V and –5000V. The complete measurement and current injection device must also be referenced to this voltage. During the measurements, all the devices are thus strongly negatively polarised.

Chapitre 5. Conclusion

The simulation of the solar array behaviour in flight configuration with respect to ESD and Secondary arcing risk allows to prove *a priori* its compatibility with geostationary charging environment.

To do so, we need to know all the physical processes leading to the secondary arcing.

It is very important to take into account :

- The response time of the power supply.
- The availability of the energy during the electrostatic discharge with respect to time.
  The structure voltage increase which drives the discharge and the energy distribution in time during an ESD of a 30nF capacitance biased at -500V(inverted voltage gradient due to plasma) will never be the same than the one delivered by a 300pF capacitance biased at -5kV (inverted voltage gradient due to electronic irradiation). Nevertheless, the energy available is the same. Be careful to the representativity of the test set-up when using plasma.
- No need to hot up the satellite capacitance with the coverglass capacitance. Tests would not have been representative any more.

But you must pay attention

- To the different values of capacitances **String, Satellite, Kapton**
- To take into account the right value of **the inductance and the resistance** of a string
- To get the wire length and the capacitances position (the nearest the sample as possible) under control.
- To simulate correctly the role of the coverglass in the neutralisation phenomenon. One solution, if we need more, is perhaps to use another electrical circuit including a capacitance (the coverglass capacitance interested in the discharge), a resistance and an inductance whose value have been calculated in order to drive the capacitance emptying.
- To the different EMC aspects.
- Transient currents measurements.
- Connect power supply structure to the sample structure

The aim of this study was to provide a solar cell test device to the industrialists representative of that which really occurs in flight on the geostationary orbit. For this, we needed to know the sequence of events which led to the failure allowing us to know which elements are indispensable and which are not (Physical model of ref[1]). Also, the device had to be as simple as possible. It is according to this principle that we designed the CNES Solar Array Simulator.

With four laboratory power supplies (two of them having low output capacitances, HP SAS type) and a simple diode connection box, it is possible to correctly simulate the operation of a string (or even of a complete section) of a solar array subsequent to a transient short circuit. This is where the difficulty laid as all phenomena occur in only a few microseconds. Lastly, with two Xantrek XRH 150-6 and two Hewlett Packard SAS 120V-4A power supplies, it is possible to select with this device any voltage value between 0 and 120V and any current between 0 and 4A which should allow us to define the criticality level of the current-voltage pair for solar arrays faced with the secondary arc triggering risk during an electrostatic discharge or during the ignition of a thruster.

Chapitre 6. References

Réf[1] Denis Payan , François Sévérin, Jean-Pierre Catani, (CNES) Jean-François Roussel, René Reulet, Daniel Sarrail, (Onera/DESP)
Electrostatic Discharges on Solar Arrays. Physical Model of Inverted Potential Gradient Electrostatic Discharge. 7th SCTC, 23-27 April 2001, Noordwijk, Nederland

Réf[2] R. Reulet, L. Levy, D. Sarrail, D. Payan.
"Décharges électrostatiques sur le générateur solaire du satellite Stentor Simulation expérimentale et définition des risques encourus." 10e Colloque International de Compatibilité Electromagnétique CEM2000 14-16 Mars 2000 Clermont-Ferrand France.

Réf[3] D. Payan.
"A model of inverted voltage gradient discharge inducing a secondary arc between cells on a solar array." European Round Table on the Modelling of S/C-Plasma Interactions 24-25 February 2000, ESA-ESTEC.

Réf[4] D Payan.
« Les décharges électrostatiques. » Cours de technologie spatiale : Techniques & Technologies des Véhicules Spatiaux.
Volume 3, Module XIII-5, pp 631-658, Cépadues Edition.

Réf[5] D Payan.
« Les décharges électrostatiques induites par l'environnement géostationnaire. » Cours de technologie Environnement spatial : Prévention des risques liés aux phénomènes de charge. pp289-329 Cépadues Edition, Toulouse Juin 1996

Réf[6] D Schwander.
« Dynamic electrical model of a Solar Array. » CNES Technical paper. To be published.